

High-Power-Efficiency Blue Electrophosphorescence Enabled by the Synergistic Combination of Phosphine-Oxide-Based Host and Electron-Transporting Materials

Shaolong Gong,^{†,§,⊥,‡} Yi-Lu Chang,^{§,‡} Kailong Wu,[†] Robin White,[§] Zheng-Hong Lu,^{*,§} Datong Song,[⊥] and Chuluo Yang^{*,†}

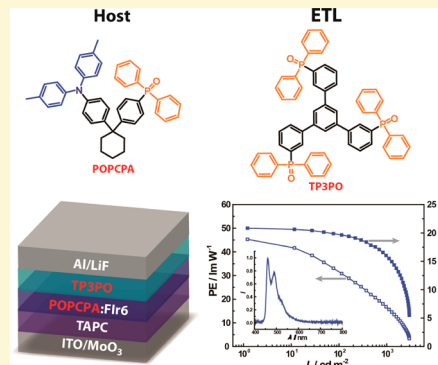
[†]Hubei Collaborative Innovation Center for Advanced Organic Chemical Materials, Hubei Key Lab on Organic and Polymeric Optoelectronic Materials, Department of Chemistry, Wuhan University, Wuhan 430072, People's Republic of China

[§]Department of Materials Science and Engineering, University of Toronto, 184 College St., Toronto, Ontario M5S 3E4, Canada

[⊥]Davenport Chemical Research Laboratories, Department of Chemistry, University of Toronto, 80 St. George Street, Toronto, Ontario M5S 3H6, Canada

Supporting Information

ABSTRACT: A new host material of (4-{1-[4-(diphenylphosphoryl)phenyl]-cyclohexyl}phenyl)bis(4-methylphenyl)amine (POPCPA) is designed and synthesized by integrating electron-donating 4,4'-dimethyldiphenylamine unit and electron-accepting diphenylphosphine oxide group into the cyclohexane skeleton. The design strategy endows the host material with a high triplet energy of 2.93 eV, a shallow HOMO level of -5.24 eV, and a bipolar charge transporting feature. In addition, a new electron-transporting (ET) material of 1,3,5-tri[3-(diphenylphosphoryl)phenyl]benzene (TP3PO), which possesses a high triplet of 2.78 eV, a deep HOMO level of -6.40 eV, and a good ET ability, is constructed by the suitable combination of three diphenylphosphine oxide groups and the triphenylbenzene skeleton. These features render these phosphine-oxide-based functional materials ideal for blue phosphorescent organic light-emitting diodes (PhOLEDs). By employing these functional materials, a blue device exhibits low driving voltages of 2.6, 3.6, and 5.4 V at the luminance of 1, 100, and 1000 cd m^{-2} , respectively, and the highest power efficiency (up to 45.3 lm W^{-1}) to date for iridium(III) bis(4',6'-difluorophenylpyridinato)-tetrakis(1-pyrazolyl)borate (FIr6)-based blue PhOLEDs, which is significantly higher than those of the FIr6-based PhOLEDs with n-doped electron-transporting layer or p-i-n structure. These results suggest that the high-power-efficiency blue PhOLEDs can be achieved by elaborate designing of host and electron-transporting materials systematically to suit the blue emitter and emission zone structure.



INTRODUCTION

Organic light-emitting diodes (OLEDs) are considered the next-generation technology for flexible flat-panel displays and low-cost general lighting sources. Phosphorescent OLEDs (PhOLEDs) are particularly attractive because the introduction of phosphors can boost the internal quantum efficiency up to 100% through the utilization of both singlet and triplet excitons.^{1–3} Although external quantum efficiencies (EQEs) over 25% have been realized for multicolor PhOLEDs without any light out-coupling enhancement,^{4–7} there is still a long way for the commercialization of PhOLEDs for solid lighting sources because of their high power consumption and poor device stability. To reduce the power consumption, two key issues need to be addressed in the enhancement of power efficiency (PE) of PhOLEDs: improving the EQE, and reducing the device driving voltage. To date, green and red PhOLEDs with high power efficiencies have been achieved,^{4a,5b,8} but high-power-efficiency blue PhOLEDs remain to be further developed.⁹ Among the blue PhOLEDs, the focus is still

placed on the typical phosphor of iridium(III) bis(4',6'-difluorophenylpyridinato)tetrakis(1-pyrazolyl)borate (FIr6).^{10–12} Since then, several research groups have endeavored to develop high-power-efficiency FIr6-based PhOLEDs through optimizing device structures.^{13,14} Xue et al. demonstrated a maximum PE of 36 lm W^{-1} by incorporating a double emitting layer into p-i-n type cell architecture;^{13b} Chu et al. reported a highly efficient FIr6-based PhOLED with a peak PE of 39.2 lm W^{-1} by utilizing the mixed host system and n-doped electron-transporting layer (ETL).^{14b}

Despite efficiency improvement, these reported FIr6-based PhOLEDs require complicated device structures that inevitably result in high driving voltages, control difficulties, and high cost, and thus restrict further enhancement of PE and the commercialization of PhOLEDs for lighting. In terms of

Received: November 12, 2013

Revised: January 20, 2014

materials, rational design of suitable functional materials for the FIr6-based PhOLEDs is a viable alternative to improve the PE without the introduction of complicated device structures.¹⁵ Because 1,1-bis[4-[*N,N*-di(*p*-tolyl)-amino]phenyl]cyclohexane (TAPC) with high triplet energy of 2.87 eV¹⁶ and good hole-transporting ability has been widely used as hole-transporting layers (HTLs) in the blue PhOLEDs,^{13b,14,15} the remaining key point has become how to develop efficient host and ET materials for high-power-efficiency blue PhOLEDs. The common requirement for host and ET materials is a higher triplet energy (E_T) than that of FIr6 (2.72 eV)¹⁰ so as to maintain effective energy transfer from host to guest, that is, confining excitons inside the emissive layer (EML). Besides this criterion, the host materials must possess bipolar charge transporting properties to balance charge transport in the EML, and well-matched highest occupied molecular orbital (HOMO) and lowest unoccupied molecular orbital (LUMO) levels with the adjacent HTL and ETL to facilitate carrier injection into the EML.^{3b,17} The ideal ET material should possess efficient ET ability to maintain the charge balance in the devices and low HOMO level to block holes.¹⁸ In this context, it becomes a significant challenge in the search of the host and ET materials that simultaneously meets all the respective requirements for high-power-efficiency blue PhOLEDs.

Recently, phosphine oxide derivatives of aromatic molecules have emerged as a new class of efficient host and ET materials for blue PhOLEDs, which showed promise in reducing the driving voltage.^{7a,19,20} Inspired by this, we design and synthesize a new host material of POPCPA by integrating electron-donating 4,4'-dimethyldiphenylamine unit and electron-accepting diphenylphosphine oxide group into the cyclohexane skeleton. As expected, the proposed host material possesses a high E_T of 2.93 eV, a shallow HOMO level of -5.24 eV, and a bipolar charge transporting feature. In addition, we also construct a new ET material of TP3PO by incorporating three diphenylphosphine oxide groups into the triphenylbenzene skeleton. The design strategy endows the ET material with a high E_T (2.78 eV), a deep HOMO level (-6.40 eV), and good ET ability. As a result, the synergistic combination of these two materials leads to a FIr6-based blue PhOLED with a peak EQE of 20.8% and low driving voltages of 2.6, 3.6, and 5.4 V at the luminance of 1 (turn-on), 100, and 1000 cd m⁻², respectively. Without any light out-coupling enhancement, the combination of high EQE and low driving voltage provides an outstanding maximum PE of 45.3 lm W⁻¹. To the best of our knowledge, this is the highest power efficiency for FIr6-based blue PhOLEDs and is even significantly higher than those of FIr6-based PhOLEDs with n-doped ETL or p-i-n structure.

EXPERIMENTAL SECTION

General Information. ¹H NMR and ¹³C NMR spectra were measured on a MECUYR-VX300 spectrometer. Elemental analyses of carbon, hydrogen, and nitrogen were performed on a Vario EL III microanalyzer. Mass spectra were measured on a Thermo Trace DSQ II GC/MS. UV-vis absorption spectra were recorded on a Shimadzu UV-2500 recording spectrophotometer. Photoluminescence (PL) and phosphorescence spectra were recorded on a Hitachi F-4500 fluorescence spectrophotometer. The PL quantum yields (PLQYs) of films were determined using a previously reported integrating sphere method²¹ with a 365 nm LED (Thor-laboratories M365L2) as the excitation source and an Ocean Optics Maya 2000

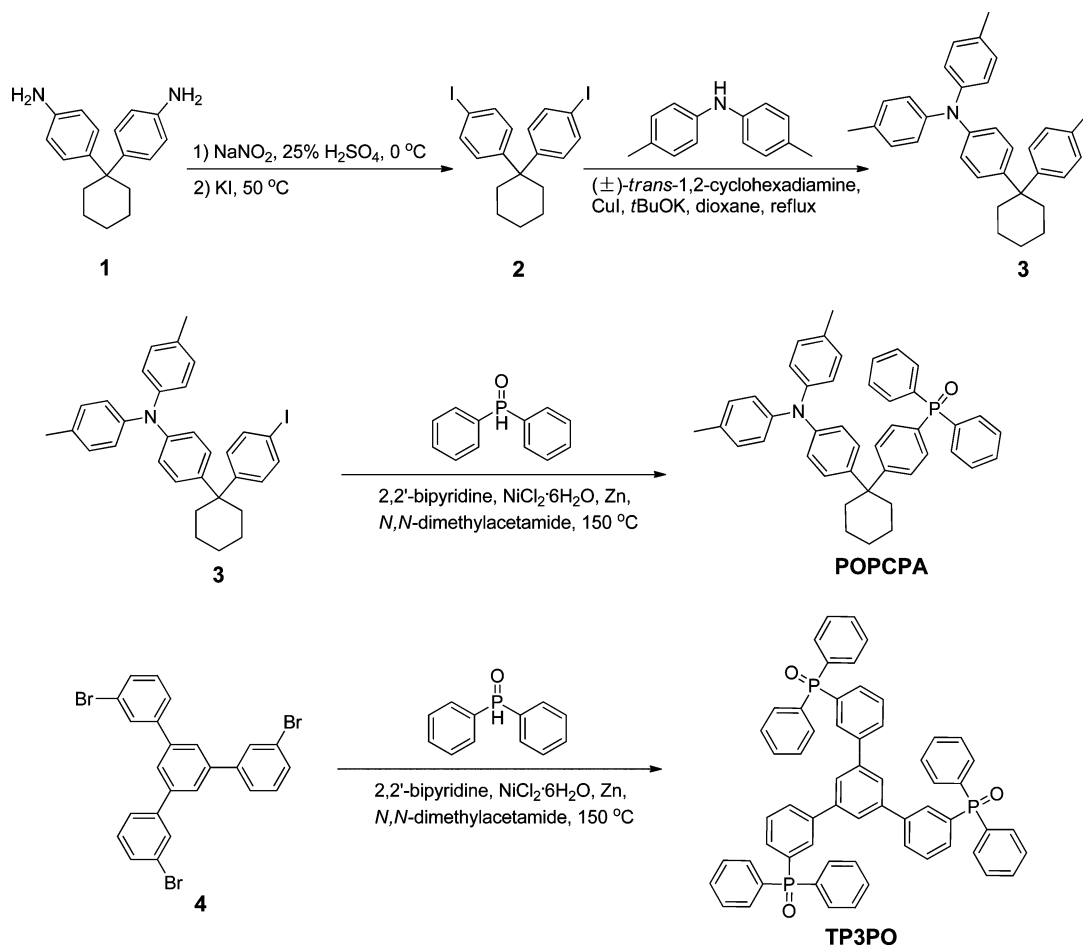
spectrometer as the optical detector. The films (50 nm thick) of codeposited host molecules and blue phosphor were formed on precleaned quartz substrates by thermal vacuum deposition (a base pressure of 10⁻⁷ Torr) and the doping concentration was 10 wt %. The absolute PLQYs were calculated by taking appropriate ratios of the excitation and emission peak areas of spectra recorded with (1) the sphere empty, (2) the excitation focused directly onto the sample, and (3) the excitation focused onto the wall of the sphere, indirectly exciting the sample. The accuracy of the system was verified against literature value for the green phosphor *fac*-tris(2-phenylpyridinato)iridium(III) (2 wt %, Ir(ppy)₃) in *N,N'*-dicarbazolyl-4,4'-biphenyl (CBP) film.^{21a} Differential scanning calorimetry (DSC) was performed on a NETZSCH DSC 200 PC unit at a heating rate of 10 °C min⁻¹ from 20 to 200 °C under argon. The glass transition temperature (T_g) was determined from the second heating scan. Thermogravimetric analysis (TGA) was undertaken with a NETZSCH STA 449C instrument. The thermal stability of the samples under a nitrogen atmosphere was determined by measuring their weight loss while heating at a rate of 10 °C min⁻¹ from 25 to 800 °C.

Device Fabrication and Measurement. The hole-injection material MoO₃ and electron-injection material LiF were purchased from Sigma-Aldrich and used as received. The hole-transporting material TAPC, host material *N,N'*-dicarbazolyl-3,5-benzene (*m*CP), electron transport materials 1,3,5-tri(*m*-pyrid-3-yl-phenyl)benzene (Tm3PyPB) and 1,3,5-tris(*N*-phenylbenzimidazol-2-yl)benzene (TPBI) were purchased from Luminescence Technology Corporation and purified by train sublimation prior to deposition. Devices were fabricated in a Kurt J. Lesker LUMINOS cluster tool with a base pressure of 10⁻⁸ Torr without breaking vacuum. The ITO anode is commercially patterned and coated on glass substrates with a thickness of 120 nm and sheet resistance of 15 Ω per square. Prior to loading, the substrate was degreased with standard solvents, blow-dried using a N₂ gun, and treated in a UV-ozone chamber. All doping concentrations used in this work are by weight percentage. The active area for all devices was 2 mm². Before removing the devices from the vacuum for characterization they were encapsulated by a 500 nm thick layer of SiO deposited by thermal evaporation. Luminance-voltage measurements were carried out using a Minolta LS-110 Luminance Meter. Current-voltage characteristics were measured using an HP4140B pA meter. The electroluminescence spectra were measured using an Ocean Optics USB4000 spectrometer calibrated with a standard halogen lamp. The radiant flux for calculating EQEs was measured using an integrating sphere equipped with an Ocean Optics USB4000 spectrometer with NIST traceable calibration using a halogen lamp.²² UPS measurements were performed using a PHI 5500 Multi-Technique system, with attached organic deposition chamber with a base pressure of 10⁻¹⁰ Torr. Additional details regarding device fabrication, characterization, and UPS measurements have been described elsewhere.²³

Materials. {4-[1-(4-Aminophenyl)cyclohexyl]phenyl}amine (1) and 1,3,5-tri(3-bromophenyl)benzene (4) were prepared according to previously reported procedures, respectively.^{24,25} The solvents were dried using standard procedures. All other reagents were used as received from commercial sources unless otherwise stated.

Synthesis of 1,1'-Cyclohexane-1,1'-diylbis(4-iodobenzene) (2). An aqueous solution (15 mL) of NaNO₂ (2.97 g, 43 mmol) was added dropwise to a stirring mixture of 1 (5.33 g, 20

Scheme 1. Synthetic Routes and Chemical Structures of POPCPA and TP3PO



mmol) in 25% H_2SO_4 (47 g, 120 mmol) at 0 °C for 1 h. After stirring at 0 °C for another 2 h, the formed suspension was dropped slowly into a stirring aqueous solution (100 mL) of KI (8.63 g, 52 mmol) at 50 °C and the reaction mixture was stirred vigorously at 50 °C for 6 h. After cooling to room temperature, the mixture was extracted with CH_2Cl_2 , washed with an aqueous $\text{Na}_2\text{S}_2\text{O}_3$ solution and brine, and dried over anhydrous Na_2SO_4 . After removal of the solvent, the residue was purified by column chromatography on silica gel using petroleum as the eluent to give a white powder. Yield: 54%. ^1H NMR (300 MHz, CDCl_3 , 25 °C, TMS): δ 7.58 (d, J = 8.7 Hz, 4H), 6.99 (d, J = 8.7 Hz, 4H), 2.21–2.17 (m, 4H), 1.57–1.50 (m, 6H). ^{13}C NMR (75 MHz, CDCl_3 , 25 °C): δ 147.84, 137.49, 129.40, 91.43, 46.02, 36.85, 26.32, 22.89. MS (EI): m/z 488.0 (M^+).

Synthesis of 4-[1-(4-Iodophenyl)cyclohexyl]phenylbis(4-methylphenyl)amine (3). A mixture of **2** (8.2 g, 16.8 mmol), 4,4'-dimethyldiphenylamine (2.36 g, 12 mmol), CuI (114 mg, 0.6 mmol), *t*BuOK (2.02 g, 18 mmol), and (\pm) -*trans*-1,2-diamino-cyclohexane (0.144 mL, 1.2 mmol) in 1,4-dioxane (30 mL) was refluxed under an argon atmosphere for 18 h. After cooling to room temperature, the reaction mixture was poured into brine, extracted with CH_2Cl_2 , washed with brine, and dried over anhydrous Na_2SO_4 . After removal of the solvent, the residue was purified by column chromatography on silica gel using dichloromethane/petroleum (1:5 by vol) as the eluent to give a white powder. Yield: 63%. ^1H NMR (300 MHz, CDCl_3 , 25 °C, TMS): δ 7.58 (d, J = 8.4 Hz, 2H), 7.06–7.02 (m, 8H), 6.95 (d, J = 8.7 Hz, 4H), 6.91–6.88 (m, 2H), 2.29 (s, 6H),

2.22–2.18 (m, 4H), 1.56–1.50 (m, 6H). ^{13}C NMR (75 MHz, CDCl_3 , 25 °C): δ 145.54, 145.31, 137.15, 132.15, 129.73, 129.44, 127.42, 124.38, 122.24, 110.82, 110.71, 90.67, 45.49, 36.88, 26.24, 22.81, 20.79. MS (EI): m/z 557.5 (M^+).

Synthesis of 4-[1-(4-(Diphenylphosphoryl)phenyl)cyclohexyl]phenylbis(4-methylphenyl)amine (POPCPA). A mixture of $\text{NiCl}_2 \cdot 6\text{H}_2\text{O}$ (84 mg, 0.35 mmol), zinc (460 mg, 7.0 mmol), 2,2'-bipyridine (112 mg, 0.72 mmol), **3** (2.0 g, 3.59 mmol), and diphenylphosphine oxide (798 mg, 3.95 mmol) in *N,N*-dimethylacetamide (20 mL) was stirred under argon at 150 °C for 48 h. After cooling to room temperature, the mixture was diluted with water, extracted with CH_2Cl_2 , and washed with brine. Then the organic phases were dried with anhydrous MgSO_4 . After removing the solvent, the residue was purified by column chromatography on silica gel using methanol/ CH_2Cl_2 (1:20 by vol) as the eluent to give a light yellow powder. Yield: 42%. ^1H NMR (300 MHz, CDCl_3 , 25 °C, TMS): δ 7.72–7.64 (m, 4H), 7.57–7.50 (m, 4H), 7.48–7.42 (m, 4H), 7.40–7.36 (m, 2H), 7.06–7.02 (m, 6H), 6.96 (d, J = 8.4 Hz, 4H), 6.90 (d, J = 8.7 Hz, 2H), 2.29 (s, 6H), 2.23–2.22 (m, 4H), 1.53–1.50 (m, 6H). ^{13}C NMR (75 MHz, CDCl_3 , 25 °C): δ 145.75, 145.39, 132.29, 132.20, 132.10, 131.90, 131.87, 129.87, 128.57, 128.45, 127.70, 127.53, 127.40, 124.56, 122.28, 46.02, 37.02, 26.35, 22.90, 20.89. MS (EI): m/z 631.7 (M^+). Anal. Calcd for $\text{C}_{44}\text{H}_{42}\text{NOP}$ (%): C, 83.65; H, 6.70; N, 2.22. Found: C, 83.52; H, 6.56; N, 2.27.

Synthesis of 1,3,5-Tri[3-(diphenylphosphoryl)phenyl]benzene (TP3PO). Prepared as a white solid according to the

same procedure as POPCPA but using 1,3,5-tri(3-bromophenyl)benzene (4). Yield: 38%. ^1H NMR (300 MHz, CDCl_3 , 25 $^\circ\text{C}$, TMS): δ 8.08 (d, J = 12 Hz, 3H), 7.80 (d, J = 6 Hz, 3H), 7.73–7.67 (m, 15H), 7.55–7.48 (m, 24H). ^{13}C NMR (75 MHz, CDCl_3 , 25 $^\circ\text{C}$): δ 141.21, 140.85, 140.71, 133.68, 132.73, 131.84, 131.34, 130.89, 130.67, 128.41, 128.27, 125.48. MS (EI): m/z 906.1 (M^+). Anal. Calcd for $\text{C}_{60}\text{H}_{45}\text{O}_3\text{P}_3$ (%): C, 79.46; H, 5.00. Found: C, 79.27; H, 4.90.

RESULTS AND DISCUSSION

Synthesis and Characterization. The synthetic routes and chemical structures of the host material of (4-{1-[4-(diphenylphosphoryl)phenyl]cyclohexyl}phenyl)bis(4-methylphenyl)amine (POPCPA) and the electron-transporting material of 1,3,5-tri[3-(diphenylphosphoryl)phenyl]benzene (TP3PO) are depicted in Scheme 1. The starting material 1 was subjected to a diazo reaction to produce 2, which was coupled with 4,4'-dimethyldiphenylamine to yield the key intermediate 3.²⁶ The desired products of POPCPA and TP3PO were prepared through cross-coupling reactions of diphenylphosphine oxide with 3 and 4, respectively.²⁷ POPCPA and TP3PO were characterized with ^1H and ^{13}C NMR spectroscopy, mass spectrometry, and elemental analysis (see the Experimental Section). POPCPA and TP3PO decompose at 406 and 525 $^\circ\text{C}$ (decomposition temperature (T_d), corresponding to 5% weight loss, determined by thermogravimetric analysis (TGA)), respectively, and display glass transition temperatures (T_g , determined by the differential scanning calorimetry (DSC)) of 90 and 123 $^\circ\text{C}$, respectively (Figure 1). Such high T_d and T_g can benefit the stability of the devices at elevated temperatures.

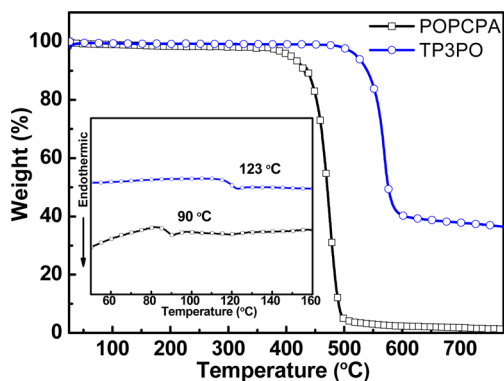


Figure 1. TGA traces of POPCPA and TP3PO recorded at a heating rate of 10 $^\circ\text{C}$ min^{-1} . Inset: DSC traces of POPCPA and TP3PO recorded at a heating rate of 10 $^\circ\text{C}$ min^{-1} .

Photophysical Properties. Absorption, fluorescence, and phosphorescence spectra of POPCPA and TP3PO are shown in Figure 2, and the key parameters are summarized in Table 1. Their bandgaps (E_g) estimated from their absorption edges in the film state (Supporting Information Figure S1) are 3.40 (POPCPA) and 3.95 eV (TP3PO). The E_T of the compounds are determined to be 2.93 (POPCPA) and 2.78 eV (TP3PO) by the highest-energy vibronic sub-band of their phosphorescence spectra in 2-methyltetrahydrofuran at 77 K, which are substantially higher than that of the blue phosphor FIr6 (2.72 eV), indicating that they can confine excitons on the blue phosphor inside the EML. To further evaluate the suitability of POPCPA as host material for blue phosphor FIr6, we measured

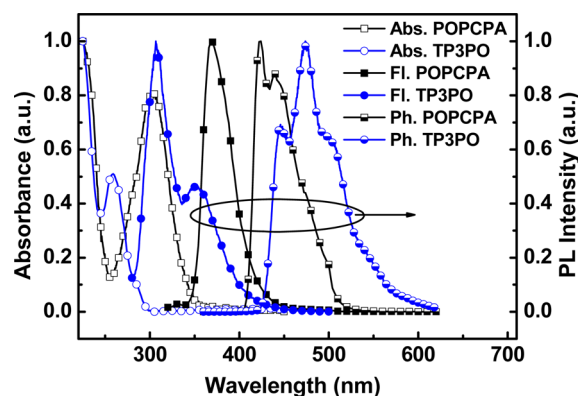


Figure 2. Normalized UV-vis absorption and fluorescence spectra of POPCPA and TP3PO in hexane at 5×10^{-6} M at room temperature, and phosphorescence spectra of POPCPA and TP3PO in 2-methyltetrahydrofuran at 77 K.

the photoluminescence quantum yield (PLQY) of the film with 10 wt % FIr6 doped in POPCPA. For comparison, we also measured the PLQY of the film with 10 wt % FIr6 doped in *m*CP. Both doped films showed relatively high PLQYs (86% for POPCPA:10 wt % FIr6 and 88% for *m*CP:10 wt % FIr6), which are indicative of potentially good host material of POPCPA for blue phosphor FIr6.

HOMO and LUMO Levels. The HOMO levels of the new compounds were probed by ultraviolet photoemission spectroscopic (UPS) measurements under a vacuum (about 10^{-10} Torr). Figure 3 panels a and b show the UPS valence band spectra (used for determining HOMO offset) and the secondary electron spectra (used for determining work function) of POPCPA and TP3PO, respectively. Our measurements show that the HOMO level of POPCPA is at -5.24 eV, which is slightly higher than that of hole-transporting material TAPC (-5.5 eV),²⁸ that is, no hole-injection barrier from TAPC to POPCPA in the device. The HOMO level of TP3PO is at -6.40 eV, suggesting that TP3PO can act as an efficient ET/hole-blocking (HB) layer in the PhOLEDs. The LUMO level of TP3PO deduced from the E_g (3.95 eV) and HOMO of TP3PO is -2.45 eV, which is suitable for electron injection from the cathode.

Electroluminescent Devices. To evaluate the charge-transporting character of POPCPA, a hole-only device having the structure of ITO/ MoO_3 (1 nm)/TAPC (60 nm)/POPCPA (70 nm)/ MoO_3 (1 nm)/Al and an electron-only device having the configuration of Al/LiF (1 nm)/POPCPA (70 nm)/TP3PO (40 nm)/LiF (1 nm)/Al were fabricated. The current density versus voltage curves show that the hole-current density is comparable to the electron-current density in POPCPA (Figure 4), indicating the bipolar transporting nature of POPCPA.

To assess the properties of POPCPA and TP3PO in electroluminescence (EL), we fabricated the FIr6-based blue device (device A) by employing these two compounds as the host and ETL materials, respectively, with the configuration of ITO/ MoO_3 (1 nm)/TAPC (60 nm)/POPCPA:10 wt % FIr6 (15 nm)/TP3PO (40 nm)/LiF (1 nm)/Al. In the device, MoO_3 and LiF were used as hole- and electron-injecting layers, respectively; TAPC and TP3PO served as the hole- and electron-transporting layers, respectively; FIr6 doped into POPCPA was used as the emitting layer. For comparison, we also fabricated the control device (device B) employing the

Table 1. Physical Data of POPCPA and TP3PO

compound	T_g^a [°C]	T_d^b [°C]	λ_{abs}^c [nm]	$\lambda_{\text{em}/\text{max}}^c$ [nm]	E_g^d [eV]	E_T^e [eV]	HOMO ^f [eV]	LUMO ^g [eV]
POPCPA	90	406	303	368	3.40	2.93	-5.24	-1.84
TP3PO	123	525	259	306, 349	3.95	2.78	-6.40	-2.45

^aObtained from DSC measurements. ^bObtained from TGA measurements. ^cMeasured in hexane. ^dDetermined from the onset of absorption in film state. ^eMeasured in 2-methyltetrahydrofuran at 77 K. ^fObtained from UPS measurements. ^gCalculated from HOMO and E_g .

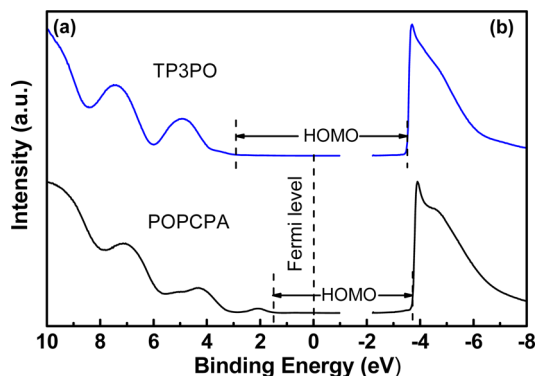


Figure 3. (a) Valence photoemission spectra of POPCPA (bottom) and TP3PO (top). (b) Secondary electron spectra of POPCPA (bottom) and TP3PO (top).

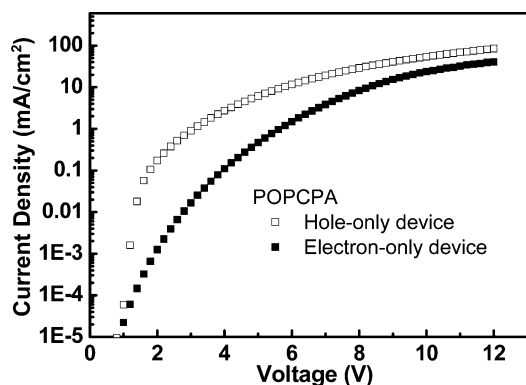


Figure 4. Current density versus voltage characteristics of the hole-only and electron-only devices. Hole-only device: ITO/MoO₃ (1 nm)/TAPC (60 nm)/POPCPA (70 nm)/MoO₃ (1 nm)/Al. Electron-only device: Al/LiF (1 nm)/POPCPA (70 nm)/TP3PO (40 nm)/LiF (1 nm)/Al.

widely used host of *m*CP for blue electrophosphorescence with the same configuration.¹⁰ The current density–voltage–luminance (*J–V–L*) characteristics and efficiency versus luminance curves for the devices are shown in Figure 5, and the key EL data are summarized in Table 2. The POPCPA-based device A showed extremely low driving voltages of 2.6, 3.6, and 5.4 V at the luminance of 1 (turn-on), 100, and 1000 cd m⁻², respectively, compared to voltages of 3.0, 4.2, and 6.2 V at the same luminance for the *m*CP-based control device B. This can be attributed to the shallower HOMO level of POPCPA (-5.24 eV) compared with that of *m*CP (-5.9 eV),¹⁰ thereby leading to no hole injection barrier from TAPC (HOMO level of -5.5 eV) to POPCPA with respect to a large injection barrier of 0.4 eV from TAPC to *m*CP. Furthermore, the low driving voltages of device A are even comparable to those of FIr6-based PhOLED with p-i-n configuration, which required 3.0, 3.4, and 4.3 V at the luminance of 0.1, 100, and 1000 cd m⁻², respectively.^{13b} Remarkably, device A shows a maximum current efficiency (CE_{max}) of 37.5 cd A⁻¹

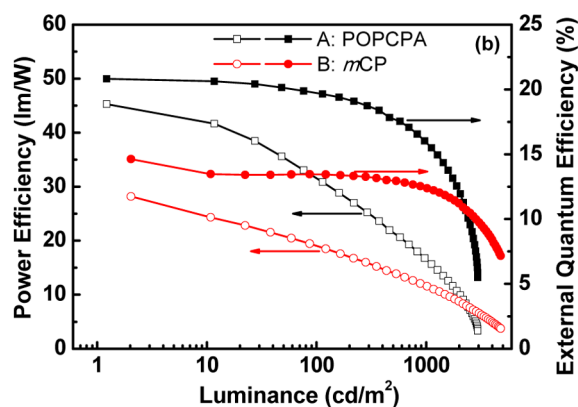
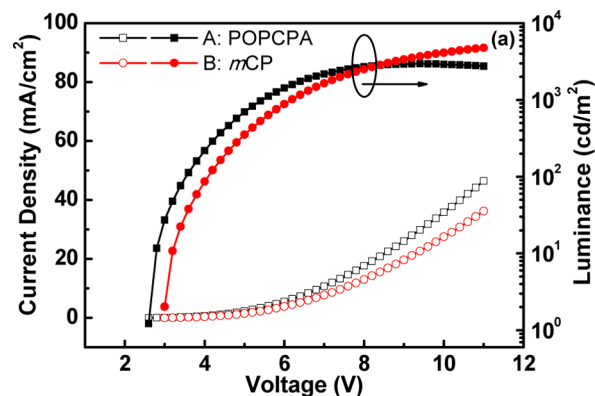


Figure 5. (a) Current density–voltage–luminance characteristics for devices A and B. (b) Power efficiency and external quantum efficiency and versus luminance curves for devices A and B.

(Supporting Information Figure S2), and a maximum EQE (EQE_{max}) of 20.8%, which is significantly higher than that of the control device B (CE_{max} of 26.9 cd A⁻¹ and EQE_{max} of 14.6%). Considering the fact that the PLQYs for the doped films are almost the same (86% for POPCPA:10 wt % FIr6 and 88% for *m*CP:10 wt % FIr6), the superior device performance of POPCPA-based device A over *m*CP-based device B could be attributed to the bipolar character of POPCPA, resulting in the balanced hole and electron transport in the EML. Without any out-coupling enhancement, the combination of low driving voltage and high EQE provides an outstanding maximum power efficiency (PE_{max}) of 45.3 lm W⁻¹ for device A. To the best of our knowledge, this is the highest power efficiency for FIr6-based blue PhOLEDs and is much higher even than those of FIr6-based PhOLEDs with n-doped ETL (PE_{max} of 39.2 lm W⁻¹)^{14b} or p-i-n structure (PE_{max} of 36 lm W⁻¹).^{13b} In addition, device A shows better color purity with CIE coordinates of (0.15, 0.26) than the control device B with CIE coordinates of (0.19, 0.28), which could be attributed to the shift of recombination zone in device B owing to the unbalanced charge transporting ability of *m*CP.

Table 2. Electroluminescence Characteristics of the Devices^a

device ^b	host	ETL	V ^c [V]	CE _{max} ^d [cd A ⁻¹]	PE _{max} ^d [lm W ⁻¹]	EQE _{max} ^d [%]	CIE (x, y) ^e
A	POPCPA	TP3PO	2.6, 3.6, 5.4	37.5	45.3	20.8	0.15, 0.26
				<i>36.7 ± 0.8</i>	<i>43.5 ± 1.8</i>	<i>20.4 ± 0.4</i>	
B	<i>m</i> CP	TP3PO	3.0, 4.2, 6.2	26.9	28.2	14.6	0.19, 0.28
				<i>26.2 ± 0.8</i>	<i>26.6 ± 1.7</i>	<i>14.2 ± 0.4</i>	
C	POPCPA	TPBI	2.8, 4.0, 7.0	12.1	12.9	6.6	0.17, 0.25
				<i>11.8 ± 0.4</i>	<i>12.5 ± 0.5</i>	<i>6.4 ± 0.2</i>	
D	POPCPA	Tm3PyPB	2.8, 3.8, 6.2	28.4	31.9	15.7	0.17, 0.26
				<i>28.2 ± 0.4</i>	<i>31.6 ± 0.4</i>	<i>15.6 ± 0.2</i>	

^aAbbreviations: ETL, electron-transporting layer; V, voltage; CE, current efficiency; PE, power efficiency; EQE, external quantum efficiency; CIE [x, y], Commission International de l'Éclairage coordinates. ^bDevice structure: ITO/MoO₃ (1 nm)/TAPC (60 nm)/Host:10 wt % FIr6 (15 nm)/ETL (40 nm)/LiF (1 nm)/Al (100 nm). ^cIn the order of onset, 100, and 1000 cd m⁻². ^dThe statistics (italic) based on 10 cells of each type. ^eMeasured at 3.6 V.

Generally, energy transfer from host to guest and direct charge trapping on dopants are two main emission mechanisms in OLEDs. A distinction between them can be made from the dependence of driving voltage on guest concentration.²⁹ For the energy transfer, current density–voltage (*J*–*V*) characteristics are not sensitive to the variation of the doping concentration, whereas for direct charge trapping, the dopants act as the shallow trapping centers, leading to a dependence of *J*–*V* characteristics on the doping concentration. To figure out the emission mechanism of device A, we fabricated four devices by changing the doping concentration of FIr6 from 5, to 10, to 15, and to 20 wt % in POPCPA with the structure of ITO/MoO₃ (1 nm)/TAPC (60 nm)/POPCPA: *x* wt % FIr6 (15 nm)/TP3PO (40 nm)/LiF (1 nm)/Al (100 nm). As shown in Figure 6, *J*–*V* characteristics are almost independent of FIr6

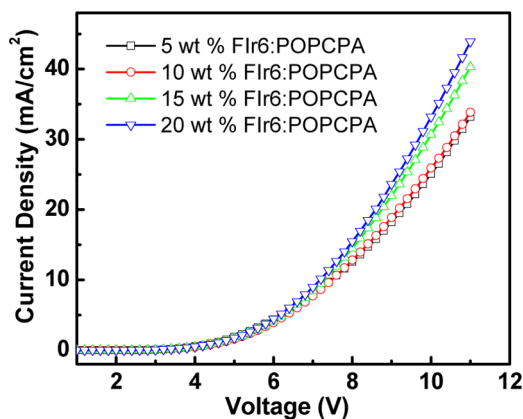


Figure 6. Current density versus voltage characteristics as a function of doping concentration in devices with the structure of ITO/MoO₃ (1 nm)/TAPC (60 nm)/POPCPA: *x* wt % FIr6 (15 nm)/TP3PO (40 nm)/LiF (1 nm)/Al (100 nm), *x* = 5, 10, 15, and 20.

concentration at the doping concentration from 5 to 10 wt %, which implies that the primary emission mechanism of FIr6 at low doping concentration (5 and 10 wt %) is the energy transfer from POPCPA to FIr6. However, in the case of the doping concentration variation from 5, to 15, and to 20 wt %, the current density increases with the increasing concentration of FIr6 at a constant driving voltage. This indicates that the primary emission mechanism of FIr6 at high doping concentration (15 and 20 wt %) is the direct charge trapping on FIr6. Therefore, for device A with 10 wt % FIr6 doped in POPCPA, the primary emission mechanism is the energy transfer from POPCPA to FIr6.

However, the excellent device performance of device A cannot completely be explained by the superiority of host material. We thought that the ETL material also plays an important role in improving device efficiencies. To figure out the contribution of ETL material to the device performance, we fabricated a set of devices based on the host of POPCPA and the widely used ETL materials of TPBI³⁰ (device C) and Tm3PyPB¹⁸ (device D), respectively. Figure 7 shows *J*–*V*–*L* characteristics and efficiency versus luminance curves for the devices C and D. Apparently, TP3PO-based device A outperforms device C (PE_{max} of 12.9 lm W⁻¹ and EQE_{max} of 6.6%) and D (PE_{max} of 31.9 lm W⁻¹ and EQE_{max} of 15.7%), which definitely indicates the superiority of TP3PO over TPBI

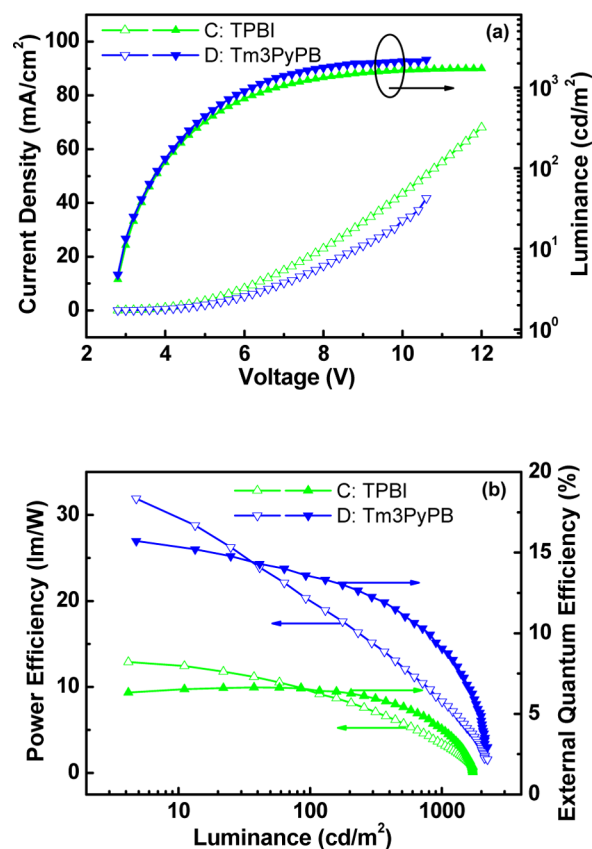


Figure 7. (a) Current density–voltage–luminance characteristics for devices C and D. (b) Power efficiency and external quantum efficiency and versus luminance curves for devices C and D.

and Tm3PyPB. To evaluate ET abilities of the three compounds, electron-only devices with a structure of Al/LiF (1 nm)/TP3PO, TPBI or Tm3PyPB (100 nm)/LiF (1 nm)/Al were constructed (Figure 8). TP3PO and TPBI showed the

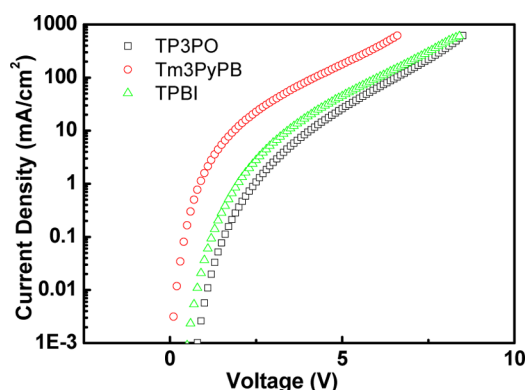


Figure 8. Current density versus voltage characteristics of the electron-only devices based on different ETL materials. Electron-only devices: Al/LiF (1 nm)/TP3PO, TPBI, or Tm3PyPB (100 nm)/LiF (1 nm)/Al.

similar electron current density under the same voltage, which is slightly lower than that of Tm3PyPB. This suggests that the ET ability of TP3PO is comparable to that of TPBI, and slightly lower than that of Tm3PyPB. On the other hand, the E_T of TP3PO (2.78 eV) is sufficiently higher than that of FIr6 (2.72 eV), indicative of the efficient exciton-confining ability of TP3PO, whereas the E_T of TPBI (2.67 eV)³⁰ or Tm3PyPB (2.75 eV)¹⁸ is lower than or close to that of FIr6 (2.72 eV), respectively, thereby possibly leading to triplet exciton quenching on TPBI or Tm3PyPB. Therefore, the excellent device performance of TP3PO-based device A surpassing those of devices C and D can be rationalized by a combination of good ET ability and high triplet energy of TP3PO.

Providing the contributions of both host and ETL materials in blue devices, the extremely high power efficiency of blue device A can be attributed to the synergistic combination of the superiorities from both the host of POPCPA and the electron-transporting material of TP3PO, that is, the matching HOMO level of POPCPA to facilitate the hole injection to the EML, the bipolar nature of POPCPA and good ET ability of TP3PO to render charge balance and a broad distribution of recombination region in the EML, and high triplet energies of POPCPA and TP3PO to ensure efficient energy transfer from the host to guest and effective exciton confinement inside the EML.

CONCLUSION

In summary, we have successfully developed two phosphine-oxide-based functional materials: POPCPA is a host material and TP3PO is an electron-transporting material. These two materials exhibit high triplet energies, appropriate HOMO levels and good charge transporting properties. By combining these two functional materials, a FIr6-based blue PhOLED exhibits low driving voltages of 2.6, 3.6, and 5.4 V at the luminance of 1, 100, and 1000 cd m⁻², respectively, and the highest PE (up to 45.3 lm W⁻¹) to date for FIr6-based blue PhOLEDs, which is significantly higher than those of the FIr6-based PhOLEDs with n-doped ETL (PE_{max} of 39.2 lm W⁻¹) or p-i-n structure (PE_{max} of 36 lm W⁻¹). This work demonstrates that the high-power-efficiency blue PhOLEDs can be achieved

by elaborate designing of host and ET materials systematically to suit the blue emitter and emission zone structure. This reported high PE should help advance the application of PhOLEDs for displays and lighting.

ASSOCIATED CONTENT

Supporting Information

Absorption spectra of POPCPA and TP3PO in film state, current efficiency versus luminance curves for devices A and B, and normalized EL spectra and CIE coordinates of devices A and B at a driving voltage of 3.6 V. This material is available free of charge via the Internet at <http://pubs.acs.org>.

AUTHOR INFORMATION

Corresponding Authors

*E-mail: clyang@whu.edu.cn. (C. Y.)

*E-mail: zhenghong.lu@utoronto.ca. (Z.-H. L.)

Author Contributions

‡These authors contributed equally.

Notes

The authors declare no competing financial interest.

ACKNOWLEDGMENTS

C.Y. thanks the National Basic Research Program of China (973 Program 2013CB834805), the Research Fund for the Doctoral Program of Higher Education of China (20120141110029), and the National Science Fund for Distinguished Young Scholars of China (51125013). Z.-H. Lu thanks the Natural Sciences and Engineering Research Council of Canada for financial support.

REFERENCES

- (1) (a) Baldo, M. A.; O'Brien, D. F.; You, Y.; Shoustikov, A.; Sibley, S.; Thompson, M. E.; Forrest, S. R. *Nature* **1998**, *395*, 151. (b) Baldo, M. A.; Lamansky, S.; Burrows, P. E.; Thompson, M. E.; Forrest, S. R. *Appl. Phys. Lett.* **1999**, *75*, 4. (c) Adachi, C.; Baldo, M. A.; Thompson, M. E.; Forrest, S. R. *J. Appl. Phys.* **2001**, *90*, 5048.
- (2) (a) Sasabe, H.; Kido, J. *Chem. Mater.* **2010**, *23*, 621. (b) Zheng, C.-J.; Ye, J.; Lo, M.-F.; Fung, M.-K.; Ou, X.-M.; Zhang, X.-H.; Lee, C.-S. *Chem. Mater.* **2012**, *24*, 643. (c) Gong, S.; Fu, Q.; Zeng, W.; Zhong, C.; Yang, C.; Ma, D.; Qin, J. *Chem. Mater.* **2012**, *24*, 3120.
- (3) (a) Xiao, L.; Chen, Z.; Qu, B.; Luo, J.; Kong, S.; Gong, Q.; Kido, J. *Adv. Mater.* **2011**, *23*, 926. (b) Tao, Y.; Yang, C.; Qin, J. *Chem. Soc. Rev.* **2011**, *40*, 2943.
- (4) (a) Fan, C.-H.; Sun, P.; Su, T.-H.; Cheng, C.-H. *Adv. Mater.* **2011**, *23*, 2981. (b) Kim, D. H.; Cho, N. S.; Oh, H.-Y.; Yang, J. H.; Jeon, W. S.; Park, J. S.; Suh, M. C.; Kwon, J. H. *Adv. Mater.* **2011**, *23*, 2721.
- (5) (a) Helander, M. G.; Wang, Z. B.; Qiu, J.; Greiner, M. T.; Puzzo, D. P.; Liu, Z. W.; Lu, Z. H. *Science* **2011**, *332*, 944. (b) Wang, Z. B.; Helander, M. G.; Qiu, J.; Puzzo, D. P.; Greiner, M. T.; Hudson, Z. M.; Wang, S.; Liu, Z. W.; Lu, Z. H. *Nat. Photonics* **2011**, *5*, 753. (c) Hudson, Z. M.; Wang, Z.; Helander, M. G.; Lu, Z.-H.; Wang, S. *Adv. Mater.* **2012**, *24*, 2922. (d) Park, Y.-S.; Lee, S.; Kim, K.-H.; Kim, S.-Y.; Lee, J.-H.; Kim, J.-J. *Adv. Funct. Mater.* **2013**, *23*, 4914.
- (6) (a) Lee, S.; Kim, K.-H.; Limbach, D.; Park, Y.-S.; Kim, J.-J. *Adv. Funct. Mater.* **2013**, *23*, 4105. (b) Su, S.-J.; Gonmori, E.; Sasabe, H.; Kido, J. *Adv. Mater.* **2008**, *20*, 4189. (c) Lee, C. W.; Lee, J. Y. *Adv. Mater.* **2013**, *25*, 5450.
- (7) (a) Jeon, S. O.; Jang, S. E.; Son, H. S.; Lee, J. Y. *Adv. Mater.* **2011**, *23*, 1436. (b) Wu, C.-A.; Chou, H.-H.; Shih, C.-H.; Wu, F.-I.; Cheng, C.-H.; Huang, H.-L.; Chao, T.-C.; Tseng, M.-R. *J. Mater. Chem.* **2012**, *22*, 17792.

- (8) (a) Tanaka, D.; Sasabe, H.; Li, Y.-J.; Su, S.-J.; Takeda, T.; Kido, J. *Jpn. J. Appl. Phys.* **2007**, *46*, L10. (b) Gong, S.; Chen, Y.; Luo, J.; Yang, C.; Zhong, C.; Qin, J.; Ma, D. *Adv. Funct. Mater.* **2011**, *21*, 1168.
- (9) (a) Gong, S.; Chen, Y.; Yang, C.; Zhong, C.; Qin, J.; Ma, D. *Adv. Mater.* **2010**, *22*, 5370. (b) Gong, S.; Chen, Y.; Zhang, X.; Cai, P.; Zhong, C.; Ma, D.; Qin, J.; Yang, C. *J. Mater. Chem.* **2011**, *21*, 11197. (c) Yook, K. S.; Lee, J. Y. *Adv. Mater.* **2012**, *24*, 3169.
- (10) (a) Holmes, R. J.; D'Andrade, B. W.; Forrest, S. R.; Ren, X.; Li, J.; Thompson, M. E. *Appl. Phys. Lett.* **2003**, *83*, 3818. (b) Ren, X.; Li, J.; Holmes, R. J.; Djurovich, P. I.; Forrest, S. R.; Thompson, M. E. *Chem. Mater.* **2004**, *16*, 4743. (c) Ye, S.; Liu, Y.; Di, C.-a.; Xi, H.; Wu, W.; Wen, Y.; Lu, K.; Du, C.; Liu, Y.; Yu, G. *Chem. Mater.* **2009**, *21*, 1333.
- (11) (a) Eom, S.-H.; Zheng, Y.; Chopra, N.; Lee, J.; So, F.; Xue, J. *Appl. Phys. Lett.* **2008**, *93*, 133309. (b) Chou, H.-H.; Cheng, C.-H. *Adv. Mater.* **2010**, *22*, 2468.
- (12) (a) Fukagawa, H.; Yokoyama, N.; Irida, S.; Tokito, S. *Adv. Mater.* **2010**, *22*, 4775. (b) Gong, S.; Fu, Q.; Wang, Q.; Yang, C.; Zhong, C.; Qin, J.; Ma, D. *Adv. Mater.* **2011**, *23*, 4956.
- (13) (a) Fukagawa, H.; Watanabe, K.; Tsuzuki, T.; Tokito, S. *Appl. Phys. Lett.* **2008**, *93*, 133312. (b) Eom, S.-H.; Zheng, Y.; Wrzesniewski, E.; Lee, J.; Chopra, N.; So, F.; Xue, J. *Org. Electron.* **2009**, *10*, 686.
- (14) (a) Lee, J.; Lee, J.-I.; Lee, J. Y.; Chu, H. Y. *Appl. Phys. Lett.* **2009**, *95*, 253304. (b) Lee, J.; Lee, J.-I.; Lee, J.-W.; Chu, H. Y. *Org. Electron.* **2010**, *11*, 1159.
- (15) Fukagawa, H.; Irida, S.; Hanashima, H.; Shimizu, T.; Tokito, S.; Yokoyama, N.; Fujikake, H. *Org. Electron.* **2011**, *12*, 1638.
- (16) Goushi, K.; Kwong, R.; Brown, J. J.; Sasabe, H.; Adachi, C. *J. Appl. Phys.* **2004**, *95*, 7798.
- (17) Chaskar, A.; Chen, H.-F.; Wong, K.-T. *Adv. Mater.* **2011**, *23*, 3876.
- (18) (a) Xiao, L.; Su, S.-J.; Agata, Y.; Lan, H.; Kido, J. *Adv. Mater.* **2009**, *21*, 1271. (b) Su, S.-J.; Takahashi, Y.; Chiba, T.; Takeda, T.; Kido, J. *Adv. Funct. Mater.* **2009**, *19*, 1260.
- (19) (a) Yu, D.; Zhao, F.; Han, C.; Xu, H.; Li, J.; Zhang, Z.; Deng, Z.; Ma, D.; Yan, P. *Adv. Mater.* **2012**, *24*, 509. (b) Sasabe, H.; Toyota, N.; Nakanishi, H.; Ishizaka, T.; Pu, Y.-J.; Kido, J. *Adv. Mater.* **2012**, *24*, 3212.
- (20) (a) Hsu, F.-M.; Chien, C.-H.; Shih, P.-I.; Shu, C.-F. *Chem. Mater.* **2009**, *21*, 1017. (b) Von Ruden, A. L.; Cosimbescu, L.; Polikarpov, E.; Koech, P. K.; Swensen, J. S.; Wang, L.; Darsell, J. T.; Padmaperuma, A. B. *Chem. Mater.* **2010**, *22*, 5678.
- (21) (a) Kawamura, Y.; Goushi, K.; Brooks, J.; Brown, J. J.; Sasabe, H.; Adachi, C. *Appl. Phys. Lett.* **2005**, *86*, 071104. (b) Endo, A.; Suzuki, K.; Yoshihara, T.; Tobita, S.; Yahiro, M.; Adachi, C. *Chem. Phys. Lett.* **2008**, *460*, 155.
- (22) Forrest, S. R.; Bradley, D. D. C.; Thompson, M. E. *Adv. Mater.* **2003**, *15*, 1043.
- (23) (a) Helander, M. G.; Greiner, M. T.; Wang, Z. B.; Lu, Z. H. *Appl. Surf. Sci.* **2010**, *256*, 2602. (b) Greiner, M. T.; Chai, L.; Helander, M. G.; Tang, W.-M.; Lu, Z.-H. *Adv. Funct. Mater.* **2012**, *22*, 4557. (c) Greiner, M. T.; Helander, M. G.; Tang, W.-M.; Wang, Z.-B.; Qiu, J.; Lu, Z.-H. *Nat. Mater.* **2012**, *11*, 76.
- (24) Yi, M. H.; Huang, W.; Jin, M. Y.; Choi, K.-Y. *Macromolecules* **1997**, *30*, 5606.
- (25) Iyer, V. S.; Wehmeier, M.; Brand, J. D.; Keegstra, M. A.; Müllen, K. *Angew. Chem., Int. Ed.* **1997**, *36*, 1604.
- (26) Klapars, A.; Antilla, J. C.; Huang, X.; Buchwald, S. L. *J. Am. Chem. Soc.* **2001**, *123*, 7727.
- (27) Zhang, X.; Liu, H.; Hu, X.; Tang, G.; Zhu, J.; Zhao, Y. *Org. Lett.* **2011**, *13*, 3478.
- (28) Kalinowski, J.; Cocchi, M.; Virgili, D.; Fattori, V.; Williams, J. A. G. *Adv. Mater.* **2007**, *19*, 4000.
- (29) (a) Uchida, M.; Adachi, C.; Koyama, T.; Taniguchi, Y. *J. Appl. Phys.* **1999**, *86*, 1680. (b) Holmes, R. J.; D'Andrade, B. W.; Forrest, S. R.; Ren, X.; Li, J.; Thompson, M. E. *Appl. Phys. Lett.* **2003**, *83*, 3818. (c) Yan, B. P.; Cheung, C. C. C.; Kui, S. C. F.; Xiang, H. F.; Roy, V. A. L.; Xu, S. J.; Che, C. M. *Adv. Mater.* **2007**, *19*, 3599.
- (30) Takizawa, S.-y.; Montes, V. A.; Anzenbacher, P., Jr. *Chem. Mater.* **2009**, *21*, 2452.